Supplementary material

Preparation of Pd/SiO_2 Catalysts by a Simple Dry Ball-milling Method for Lean Methane Oxidation and Probe of the State of Active Pd Species

Li Yang,[1,2] Chao Fan,[1,2] Li Luo,[1,2] Yanyan Chen,[1] Zhiwei Wu,[1,*] Zhangfeng Qin,[1,*] Mei Dong,[1] Weibin Fan,[1] Jianguo Wang[1,2,*]

[1] State Key Laboratory of Coal Conversion, Institute of Coal Chemistry, Chinese Academy of Sciences, P.O. Box 165, Taiyuan, Shanxi 030001, PR China

[2] University of the Chinese Academy of Sciences, Beijing 100049, PR China

[*] Correspondence. Tel.: +86-351-4046092; Fax: +86-351-4041153. E-mail address: qzhf@sxicc.ac.cn (Z. Qin); wuzhiwei@sxicc.ac.cn (Z. Wu); iccjgw@sxicc.ac.cn (J. Wang)

As the Supplementary material of the manuscript "*Preparation of Pd/SiO_2 catalysts by a simple dry ball-milling method for lean methane oxidation and probe of the state of active Pd species*", following Tables and Figures are provided:

A comparison of various supported palladium catalysts in their activity for lean methane oxidation; TEM images, Pd particle size distribution curves and XRD patterns of the Pd/SiO_2 catalysts prepared by the dry ball-milling method with different Pd precursors and treated under different conditions; FT-IR spectra of the SiO_2 support and Pd/SiO_2-Acac catalyst; TG-MS profiles of the $Pd(Acac)_2/SiO_2$ catalyst; more light off test results for lean methane oxidation; Pd 3d XPS spectra of the PdO_x/SiO_2-Acac catalysts with different Pd oxidation states; DFT calculation method and results for the dissociation of methane on the Pd^0, PdO_x and PdO species.

Table S1. A comparison of various supported palladium catalysts in their activity for lean methane combustion

Catalyst	Loading method	Reaction conditions	Pd loading (wt. %)	$T_{90\%}$ (°C)	Ref.
Pd/H-ZSM-5	impregnation	2% CH_4 + 8% O_2; GHSV = 48,000 h^{-1}	1.0	400	[1]
Pd/H-ZSM-5	deposition	1% CH_4 + 20% O_2; GHSV = 15,000 mL g^{-1} h^{-1}	0.77	311	[2]
Pd-SSZ-13	ion exchange	0.15% CH_4 + 5% O_2; GHSV = 100,000 h^{-1}	1.1	362	[3]
Pd-ZSM-5	ibid	ibid	1.30	384	[3]
Pd-H-Mordenite	ion-exchange	1% CH_4 + 99% air; GHSV = 100,000 h^{-1}	0.70	495	[4]
Pd-H-Y	ibid	ibid	1.0	475	[4]
Pd-H-SAPO-5	ibid	ibid	0.96	480	[4]
Pd/H-MCM-41	wet impregnation	O_2/CH_4 = 4; GHSV = 15,000 mL g^{-1} h^{-1}	0.98	454	[5]
Pd/MCM-48	ibid	ibid	1.05	483	[5]
Pd/H-ZSM-5	sol-gel	1% CH_4 + 99% air; GHSV = 30,000 mL g^{-1} h^{-1}	0.92	298	[6]
Pd/γ-Al_2O_3	wet impregnation	1% CH_4 + 20% O_2; GHSV = 30,000 mL g^{-1} h^{-1}	0.4	350	[7]
Pd/CeO_2	solution combustion	0.5% CH_4 + 2% O_2; GHSV = 200,000 h^{-1}	1.0	490	[8]
Pd/Co_3O_4	wet impregnation	1% CH_4 + 8% O_2; GHSV = 12,000 h^{-1}	0.79	500	[9]
Pd/SiO_2	impregnation	1% CH_4 + 99% air; GHSV = 48,000 h^{-1}	1.0	860	[10]
Pd/TiO_2	ibid	ibid	1.0	885	[10]
Pd/SnO_2	ibid	ibid	1.0	440	[10]
Pd/ZrO_2	ibid	ibid	1.0	490	[10]
Pd/In_2O_3	ibid	ibid	1.0	590	[10]
Pd/Ga_2O_3	ibid	ibid	1.0	815	[10]
Pd/Nb_2O_5	ibid	ibid	1.0	875	[10]
Pd/Y_2O_3	ibid	ibid	1.0	700	[10]

Catalyst	Loading method	Reaction conditions	Pd loading (wt. %)	$T_{90\%}$ (°C)	Ref.
Pd/SiO_2-Acac	dry ball-milling	GHSV = 30,000 mL g^{-1} h^{-1}	1.00	288	this work
Pd/SiO_2-OAc	ibid	GHSV = 30,000 mL g^{-1} h^{-1}	1.02	305	this work
Pd/SiO_2-Cl	ibid	GHSV = 30,000 mL g^{-1} h^{-1}	0.98	345	this work
Pd/SiO_2-NO_3	ibid	GHSV = 30,000 mL g^{-1} h^{-1}	1.03	462	this work

Note: $T_{90\%}$ denotes the temperature for lean methane combustion at which a methane conversion of 90% can be achieved.

Table S2. DFT calculated structures of the reactant, transition state, and product for the dissociation of methane over the Pd(100), $PdO_{0.75}$ (3ML-PdO(101)/Pd(100)), and PdO(100) surfaces as well as the corresponding energy barrier ($\Delta E_{int}^{\neq}$, eV) and reaction energy change (ΔE_r, eV)

Pd surface	Reactant	Transition state	Product	$\Delta E_{int}^{\neq}$	ΔE_r
Pd(100)	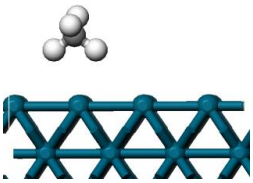	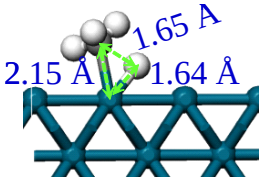	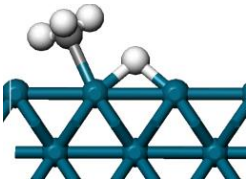	0.76	0.53
3ML-PdO(101)/Pd(100)	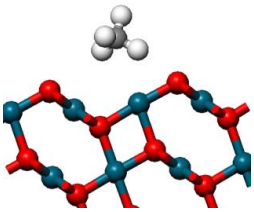	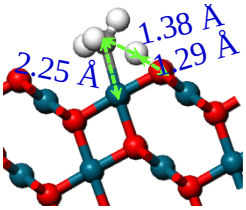	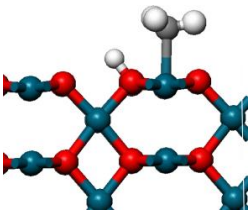	0.73	−0.33
PdO(100)	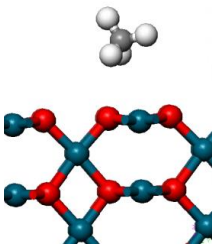	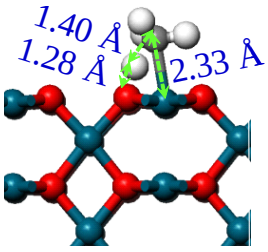	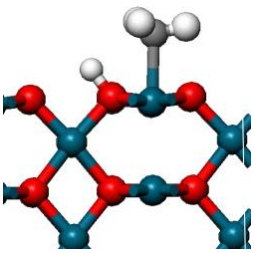	1.27	−0.05

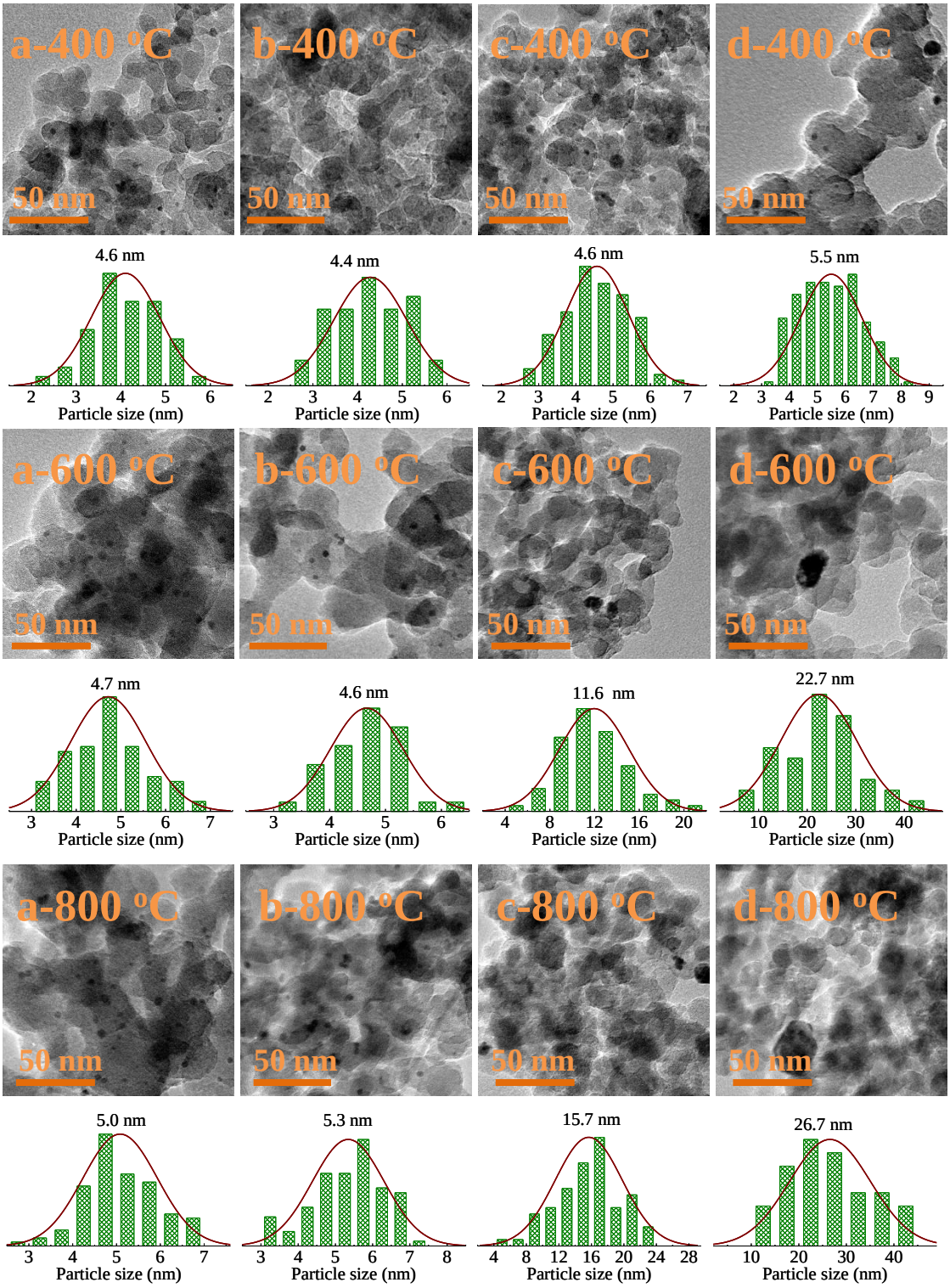

Figure S1. TEM images and Pd particle size distribution curves of the Pd/SiO_2-*x* catalysts prepared by the dry ball-milling method with different Pd precursors calcined at 400, 600 and 800 °C: (a) Pd/SiO_2-Acac, (b) Pd/SiO_2-OAc, (c) Pd/SiO_2-Cl and (d) Pd/SiO_2-NO_3.

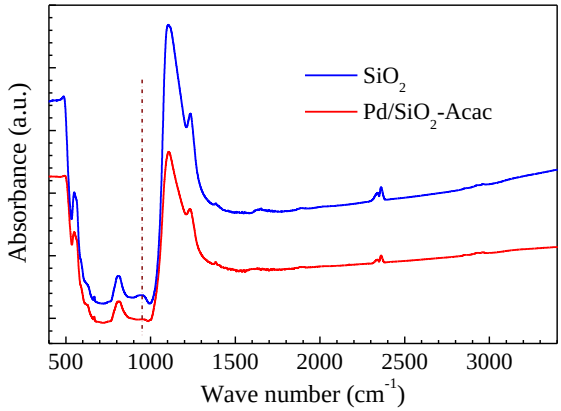

Figure S2. FT-IR spectra of the SiO_2 support and Pd/SiO_2-Acac catalyst.

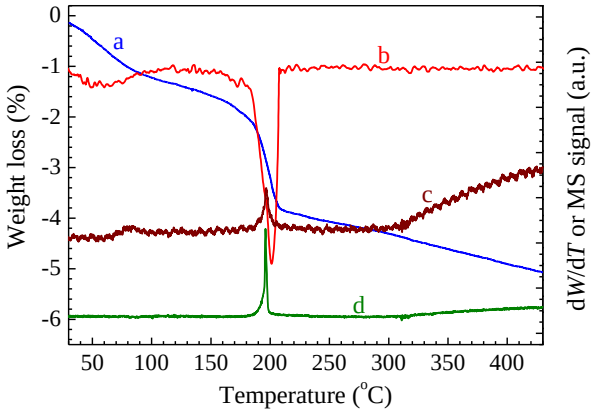

Figure S3. TG-MS profiles of the $Pd(Acac)_2/SiO_2$ catalyst: (a) weight loss; (b) DTG curve; (c) H_2O signal in effluent; (d) CO_2 signal in effluent.

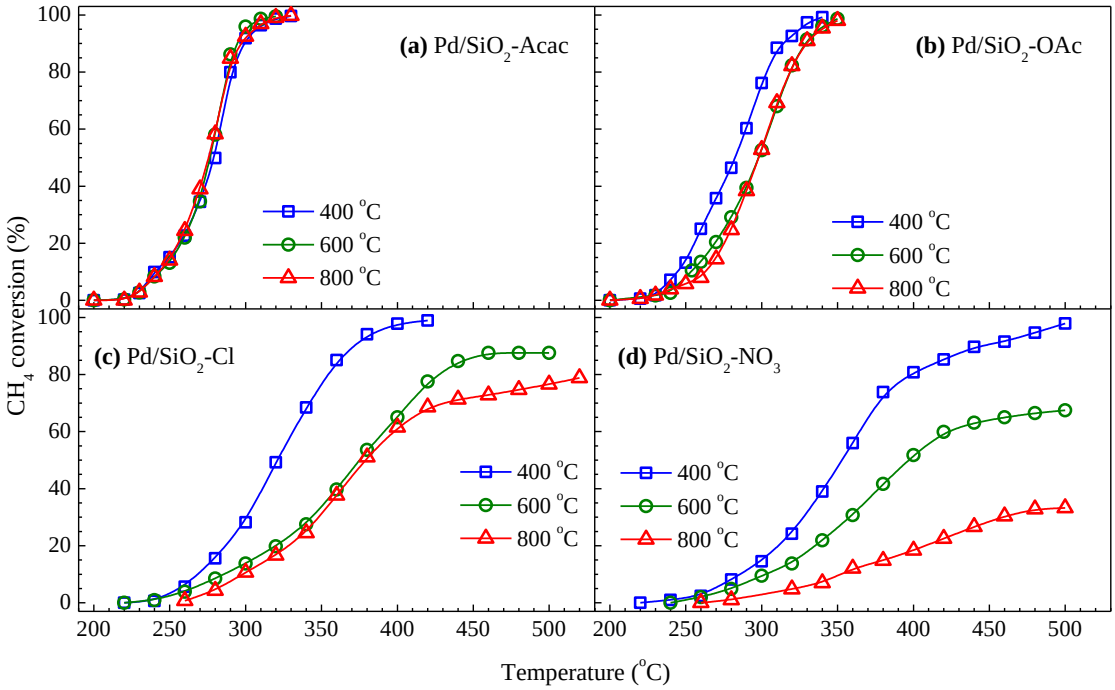

Figure S4. Light off tests of lean methane oxidation over the Pd/SiO_2-*x* catalysts prepared by the dry ball-milling method with different Pd precursors (After the ball-milling, the Pd/SiO_2 catalysts was calcined in air at 400, 600, and 800 °C, as marked in the legends, for 4 h and then reduced with hydrogen at 400 °C for 1 h): (a) Pd/SiO_2-Acac, (b) Pd/SiO_2-OAc, (c) Pd/SiO_2-Cl; and (d) Pd/SiO_2-NO_3.

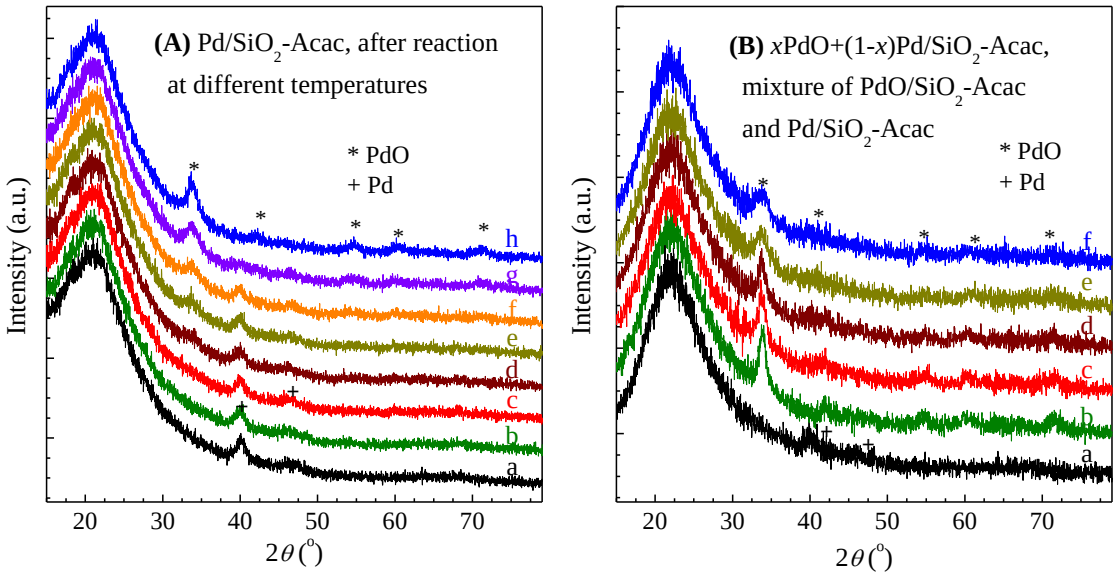

Figure S5. (**A**) XRD patterns of the Pd/SiO_2-Acac catalysts come through the lean methane oxidation reaction at different temperatures: (a) original; (b) 200 °C; (c) 220 °C; (d) 240 °C; (e) 260 °C; (f) 280 °C; (g) 300 °C; (h) 320 °C. (**B**) XRD patterns of the *x*PdO+(1−*x*)Pd/SiO_2-Acac catalysts, a mixture of PdO/SiO_2-Acac and Pd/SiO_2-Acac with different contents of PdO: (a) Pd/SiO_2-Acac; (b) 0.2PdO+0.8Pd/SiO_2-Acac; (c) 0.4PdO+0.6Pd/SiO_2-Acac; (d) 0.6PdO+0.4Pd/SiO_2-Acac; (e) 0.8PdO+0.2Pd/SiO_2-Acac; (f) PdO/SiO_2-Acac.

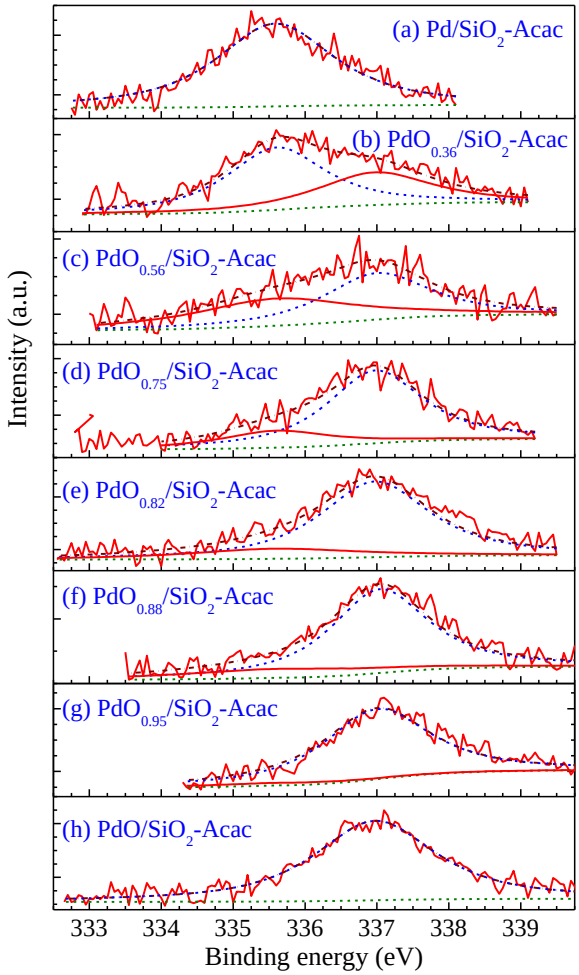

Figure S6. Pd 3d XPS spectra of the PdO_x/SiO_2-Acac catalysts with different Pd oxidation states obtained by oxidizing the previously reduced Pd/SiO_2-Acac in air for 30 min at different temperatures: (a) fresh reduced Pd/SiO_2-Acac; (b) 240 °C; (c) 250 °C; (d) 300 °C; (e) 350 °C; (f) 400 °C; (g) 500 °C; (h) calcined PdO/SiO_2-Acac.

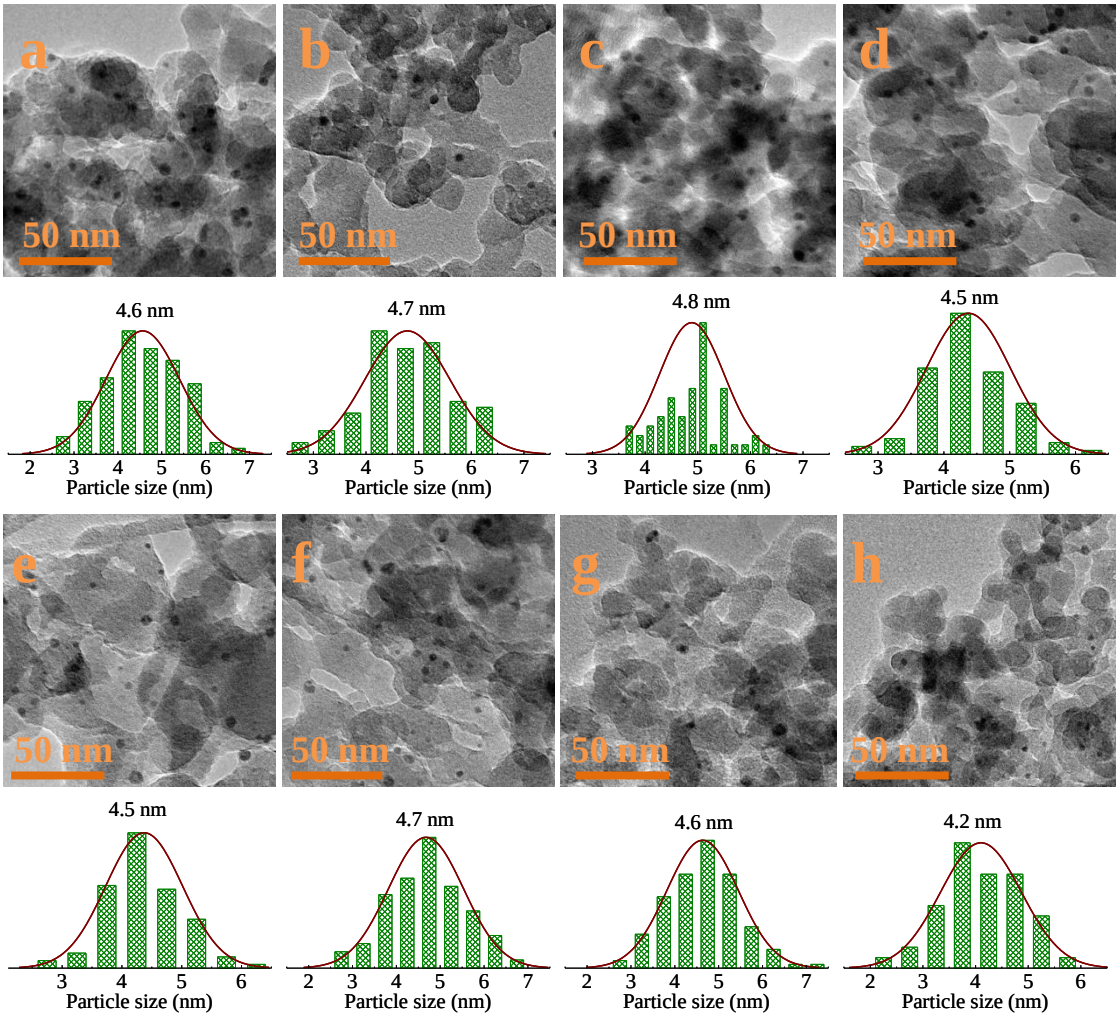

Figure S7. TEM images and Pd particle size distribution curves of the PdO_x/SiO_2-Acac catalysts with different Pd oxidation states (obtained by oxidizing the previously reduced Pd/SiO_2-Acac in air for 30 min at different temperatures): (a) Pd/SiO_2-Acac; (b) $PdO_{0.36}/SiO_2$-Acac; (c) $PdO_{0.58}/SiO_2$-Acac; (d) $PdO_{0.75}/SiO_2$-Acac; (e) $PdO_{0.82}/SiO_2$-Acac; (f) $PdO_{0.88}/SiO_2$-Acac; (g) $PdO_{0.95}/SiO_2$-Acac; (h) PdO/SiO_2-Acac.

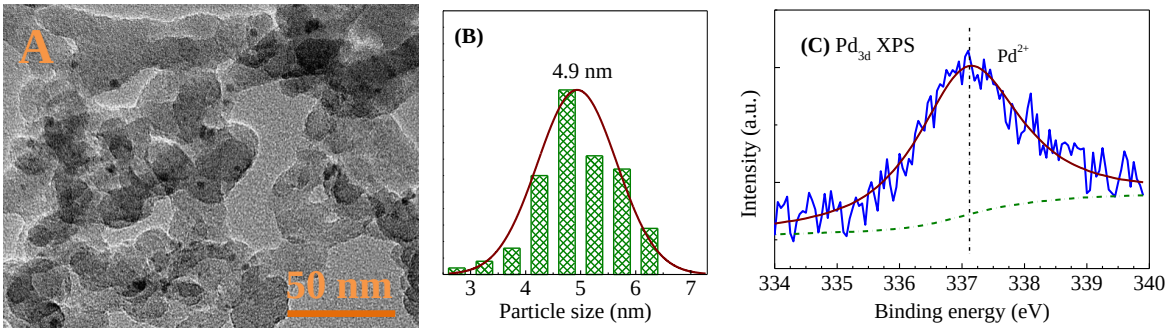

Figure S8. TEM images (**A**), Pd particle size distribution curve (**B**) and Pd 3d XPS spectra (**C**) of the spent $PdO_{0.82}/SiO_2$-Acac catalyst come through lean methane oxidation reaction at 280 °C for 60 h.

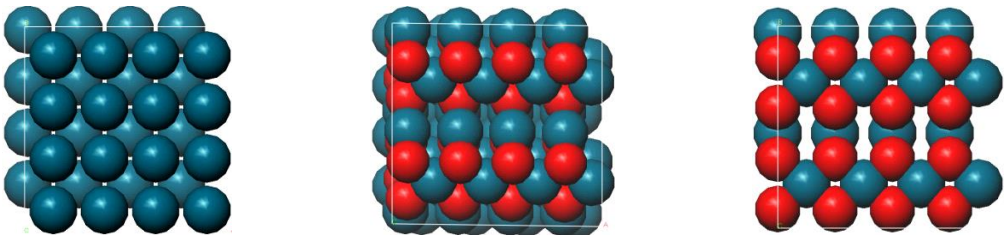

Pd(100) **3ML-PdO(101)/Pd(100)** **PdO(100)**

Figure S9. Models of the most stable bulk PdO(100), Pd(100), and 3 monolayer PdO(101)/Pd(100) (3ML, labeled as $PdO_{0.75}$, where the atomic ratio of Pd and O is 0.75). Vacuum thickness of 15 Å was used to separate the slab in the *z* directions, which was found sufficient to avoid electronic coupling between the adjacent slabs. For geometry optimization, the atoms in two lower rows were fixed and other atoms at both edge surfaces are allowed to relax.

All calculations were conducted by using the periodic plane-wave DFT methods, implemented in the Vienna ab-initio simulation program (VASP) [11]. The spin-polarization within the generalized gradient approximation (GGA) using the Perdew-Wang 91 (PW91) exchange-correlation potential and ultrasoft pseudopotentials (US-PP) was employed to describe the interactions between core and valence electrons [11,12]. As revealed previously, the U parameter in GGA+U did not significantly influence the barriers for C–H bond activation [13].Wave functions were constructed from the periodic plane-wave expansions out to a kinetic energy cutoff of 400 eV. A 2 × 2 × 1 Monkhorst−Pack k-point mesh was used

to sample the first Brillouin zone, allowing convergence to 0.1 meV of the total electronic energy and below 0.05 eV/Å of the remain total force. All transition states reported herein were isolated by using the climbing image-nudged elastic band (CI-NEB) methods [14].

References

1. Shi, C.; Yang, L.; He X.; Cai, J. Enhanced activity and stability of Zr-promoted Pd/HZSM-5 catalyst for low-temperature methane combustion. *Chem. Commun.* **2002**, *18*, 2006–2007.
2. Lou, Y.; Ma, J.; Hu W.; Lu, G. Low-Temperature Methane Combustion over Pd/H-ZSM-5: Active Pd Sites with Specific Electronic Properties Modulated by Acidic Sites of H-ZSM-5. *ACS Catal.* **2016**, *6*, 8127–8139.
3. Lim, J.; Jo D.; Hong, S. Palladium-exchanged small-pore zeolites with different cage systems as methane combustion catalysts. *Appl. Catal. B: Environ.* **2017**, *219*, 155–162.
4. Yusaku, T.; Tatsumi, I.; Hiroyasu N.; Hideaki, S. Palladium ion-exchanged SAPO-5 for a low temperature combustion of CH_4. *Stud. Surf. Sci. Catal.* **1997**, *105*, 1647–1654.
5. Ruiz, J.; Oliveira, E.; Fraga M.; Pastore, H. Performance of Pd supported on mesoporous molecular sieves on methane combustion. *Catal. Commun.* **2012**, *25*, 1–6.
6. Fan, C.; Yang, L.; Luo, L.; Wu, Z.; Qin, Z.; Zhu, H.; Fan W.; Wang, J. A highly active Pd/H-ZSM-5 catalyst in lean methane combustion prepared via a sol–gel method and treated by reduction–oxidation. *New J. Chem.* **2020**, *44*, 3940–3949.
7. Zou, X.; Rui, Z.; Song S.; Ji, H. Enhanced methane combustion performance over $NiAl_2O_4$-interface-promoted Pd/γ-Al_2O_3. *J. Catal.* **2016**, *338*, 192–201.
8. Colussi, S.; Gayen, A.; Camellone, M.F.; Boaro, M.; Llorca, J.; Fabris S.; Trovarelli, A. Nanofaceted Pd-O Sites in Pd-Ce Surface Superstructures: Enhanced Activity in Catalytic Combustion of Methane. *Angew. Chem. Int. Ed.* **2009**, *48*, 8481–8484.
9. Ercolino, G.; Stelmachowski, P.; Grzybek, G.; Kotarba A.; Specchia, S. Optimization of Pd catalysts supported on Co_3O_4 for low-temperature lean combustion of residual methane. *Appl. Catal. B: Environ.* **2017**, *206*, 712–725.
10. Sekizawa, K.; Widjaja, H.; Maeda, S.; Ozawa Y.; Eguchi, K. Low temperature oxidation of methane over Pd catalyst supported on metal oxides. *Catal. Today* **2000**, *59*, 69–74.
11. Kresse G.; Hafner, J. Ab initio molecular dynamics for liquid metals. *Phys. Rev. B* **1993**, *47*, 558–561.

12. Vanderbilt, D. Soft self-consistent pseudopotentials in a generalized eigenvalue formalism. *Phys. Rev. B* **1990**, *41*, 7892–7895.

13. Chin, Y.; Buda, C.; Neurock M.; Iglesia, E. Consequences of Metal−Oxide Interconversion for C−H Bond Activation during CH_4 Reactions on Pd Catalysts. *J. Am. Chem. Soc*. **2013**, *135*, 15425–15442.

14. Henkelman, G.; Uberuaga B.; Jónsson, H. A climbing image nudged elastic band method for finding saddle points and minimum energy paths. *J. Chem. Phys.* **2000**, *113*, 9901–9904.